Optik - International Journal for Light and Electron Optics 264 (2022) 169409

Contents lists available at ScienceDirect

Optik

journal homepage: www.elsevier.com/locate/ijleo

Switchable two-wavelength emission using vertical external-cavity surface-emitting laser

Zhang Zhuo [a,b], Zhang Jianwei [a,*], Zhang Jiye [a], Zeng Yugang [a], Zhang Jun [a], Zhou Yinli [a], Zhang Xing [a], Qin Li [a], Liu Yun [a], Ning Yongqiang [a], Wang Lijun [a]

[a] State Key Laboratory of Luminescence and Applications, Changchun Institute of Optics, Fine Mechanics and Physics, Chinese Academy of Sciences, Changchun, Jilin 130033, China
[b] University of Chinese Academy of Sciences, Beijing 100049, China

ARTICLE INFO

Keywords:
Vertical external-cavity surface-emitting laser
Quantum wells
Dual wavelength
Switchable wavelengths
InGaAs

ABSTRACT

We present an optically pumped vertical external-cavity surface-emitting laser (VECSEL) that can emit two switchable wavelengths from a single chip, with a wavelength separation of more than 40 nm. Quantum wells with two gain wavelengths are used in the active region of the gain chip. The Fabry–Perot dips in the reflectivity spectra of the VECSEL are designed to support two wavelengths. The VECSEL can simultaneously emit wavelengths of 955 and 997 nm at the pump power of 15.4–16 W; the maximum dual-wavelength output power is ~250 mW. The emitting wavelength can be switched between 950 and 1004 nm as the pumping power is changed. The output power exceeds 280 and 500 mW at 955 and 1004 nm, respectively, mainly because of the internal self-heating generated by the optical pumping process, which can quickly change the temperature of the gain chip and cause redshift of the gain peak. The temperature rise of the gain chip can change the offset between the gain peak and cavity mode, thereby changing the output wavelength.

1. Introduction

Vertical external-cavity surface-emitting lasers (VECSELs) can provide high power outputs with excellent beam quality in a simple and compact setup [1–3]. The unique external cavity structure of a VECSEL, coupled with a mature semiconductor band engineering design, can cover a wide range of wavelengths, from visible to near-infrared light [4,5]. Further, UV output can be achieved by inserting a nonlinear crystal into the external cavity of a VECSEL for frequency doubling [6]. By placing two different quantum wells (QWs) in the gain region of the VECSEL, a dual-wavelength output can be obtained from a single chip [7]. A VECSEL can emit two wavelengths from a single chip and can effectively extend the output wavelength to the terahertz frequency band through difference frequency generation [8]. Terahertz waves offer many advantages, such as low photon energy, high resolution, and strong transmission ability, which can be utilized in astronomy, life sciences, and information technology [9–12]. Recently, terahertz radiation based on difference frequency generation has been widely reported. By inserting various optical devices in the resonant cavity and adding an external modulation, the dual-wavelength vector laser can achieve fine adjustable control between dual wavelengths [13]. Although this VECSEL could achieve tunable terahertz emission, the optical device is very complex. A T-shaped cavity composed of two gain chips can also realize terahertz emission through differential frequency [14]; however, it requires two separate pump light

* Corresponding author.
E-mail address: zjw1985@ciomp.ac.cn (Z. Jianwei).

https://doi.org/10.1016/j.ijleo.2022.169409
Received 21 February 2022; Received in revised form 3 May 2022; Accepted 27 May 2022
Available online 31 May 2022

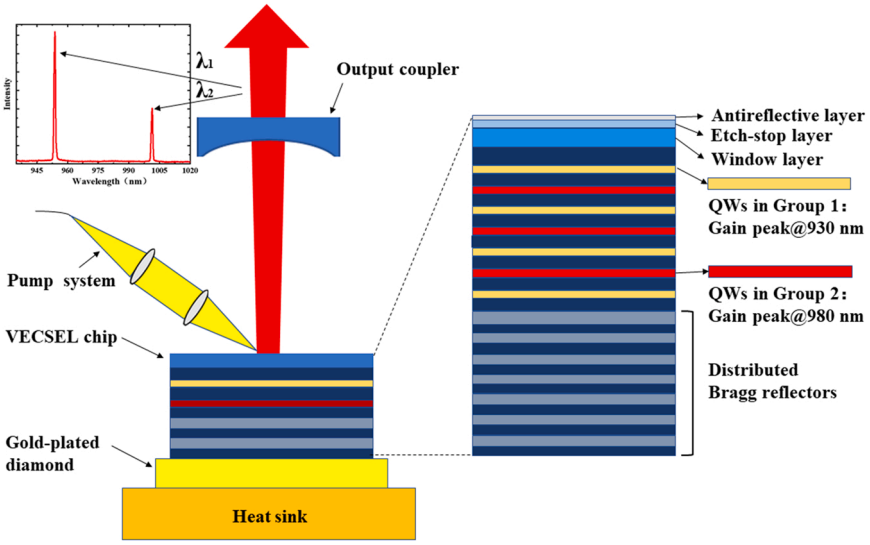

Fig. 1. Schematic of the developed VECSEL and its components. Inset: magnified view of the gain-chip structure.

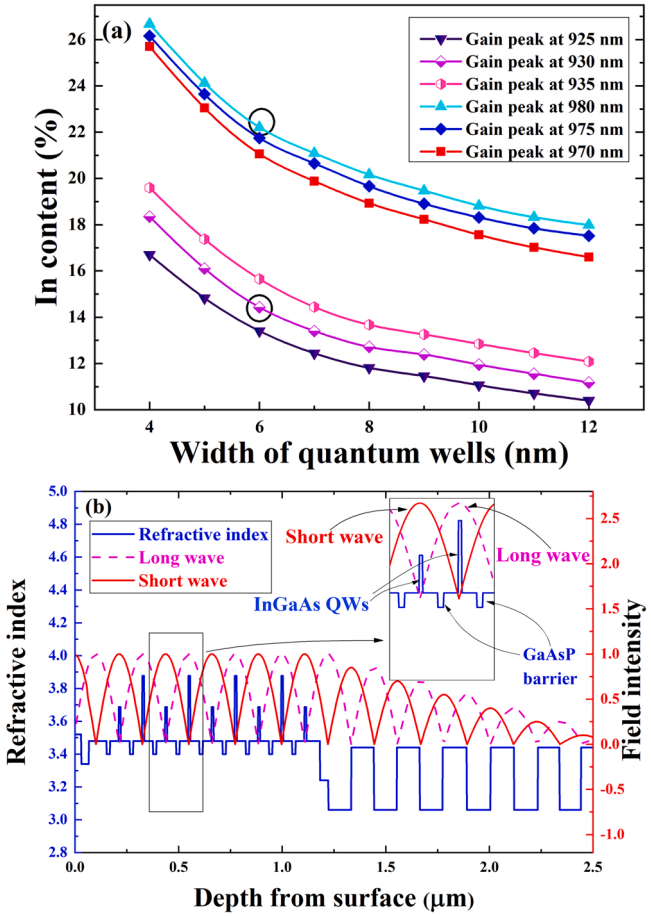

Fig. 2. (a) Relationship between In content and QW width for the emitting wavelengths of 925, 930, 935, 970, 975, and 980 nm. (b) Simulated standing-wave distribution within the gain chip of the VECSEL.

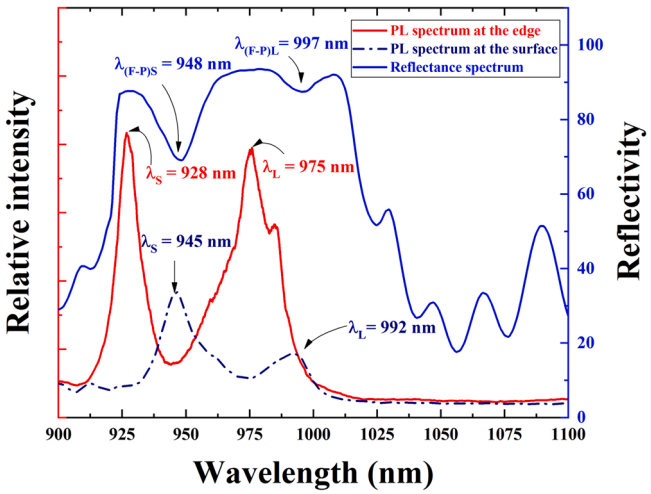

Fig. 3. Reflectivity spectrum of the gain chip after removing the substrate (blue solid line), and the photoluminescence (PL) spectra at the edge (red solid line) and surface (black dashed line) of the gain chip. The heat sink temperature is controlled at −5 °C.

sources, and the efficiency is low. Terahertz output with very low conversion efficiency can be realized by using the etalon to realize dual wavelength in the resonant cavity and inserting a difference frequency crystal [15]. Dual wavelength emission can be realized using a multi folded cavity as well, which has the potential to generate waves in the terahertz band [16].

The key requirement for realizing terahertz waves is an efficient radiation source. Different setups are used to realize multi-wavelength emission separately to generate terahertz waves through difference frequency generation [17–19]. The generation of two or more wavelengths from different gain chips in a coaxial cavity has also been demonstrated recently [20,21]. However, a two-wavelength emission from a single chip is considered to be a more effective terahertz source.

Therefore, in this study, a VECSEL capable of emitting two switchable wavelengths from a single gain chip was developed. Through the simulation of the InGaAs QW thickness and Indium composition, two QWs with different emission wavelengths were selected and placed at the belly of the corresponding standing wave. The optical cavity of the gain chip was designed to match the two wavelengths. The separation between the two wavelengths could reach 40 nm. By increasing the pumping power, the emitted wavelength from the VECSEL could be switched from 955 nm to 997 nm. The two wavelengths could also be emitted simultaneously, with the corresponding output power under dual-wavelength lasing reaching nearly 250 mW.

2. Experimental details

Fig. 1 shows the experimental configuration used in the study, which is a linear cavity design. The gain chip comprises an etch-stop layer, AlGaAs window layer, active region, and high reflection distribution Bragg reflector (DBR) (Fig. 1). The gain chip is welded to the gold-plated diamond heat sink and then installed on the copper radiator cooled by a thermoelectric cooler (TEC). Closed-cycle water cooling is used to dissipate the excess heat from the TEC. The temperature of the cooling water is set at 15 ℃. An 808 nm fiber-coupled diode laser is used as the pump source, and the beam is focused on the chip surface through two convex lenses, as shown in Fig. 1. The angle between the pump system and gain chip is nearly 45°. The pump spot size of the pump system on the surface of the gain chip is ~400 μm. Based on stability calculations of the linear cavity, the spot size of the output coupler feedback to the gain chip is matched with the pump plate, and stable straight cavity output can be achieved [22]. The spot size of the pump light and the distance between the output coupling mirror and the gain chip can be varied to obtain the best output. In the linear cavity of the laser, a concave mirror with a curvature radius of − 75 mm is used. The transmission rate of the mirror is 3%.

The gain chip is grown on GaAs (100) substrates using an Aixtron 200/4 metal organic chemical vapor deposition system. A typical “bottom-emitter” structure was utilized in this study [23]. The active region is grown on top of an GaInP etch-stop layer and a 30-nm-thick AlGaAs window layer. The AlGaAs window layer can prevent the surface accumulation effect of photogenerated carriers. Two sets of compressively strained InGaAs QWs are used in the gain chip, and the gain peaks of the QWs are designed for two different wavelengths, 930 and 980 nm. Fig. 2(a) shows the calculated In content and the corresponding thickness of the InGaAs QWs at different gain-peak wavelengths. Both the In content and QW thickness should be adjusted to maintain the gain-peak wavelength. For a fixed In content, increasing the QW width can redshift the gain-peak wavelength due to the reduced energy-band splitting of the QWs [24]. However, if the width of the quantum well is very high, the separation of the first and the second energy levels will be insufficient, and the gain peak will decrease in height [25]. Excessive In content in the quantum well would lead to an increase in material strain and affect the growth quality of the material. To realize a more accurate wavelength and better material growth quality, the width of the quantum well is selected as 6 nm, and gain peaks at 930 and 980 nm are achieved for the 14.5% and 22% components, respectively.

A GaAs layer exists on both sides of the InGaAs QWs as an optical absorption layer to absorb the pump light, and a GaAsP strain

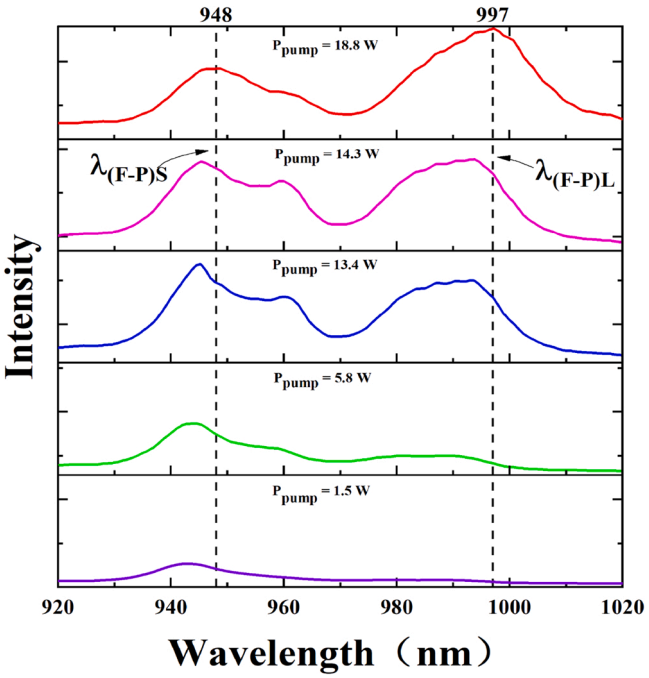

Fig. 4. PL spectra from the surface of the gain chip under different pump powers. The heat sink temperature is controlled at −5 °C.

compensation layer exists on the GaAs layer to compensate for material strain [26]. The optical cavity of the gain chip is specially designed to support two lasing wavelengths of 950 nm and 1000 nm [27]. Moreover, the QWs are placed in the antinodes of a standing-wave pattern to achieve effective coupling between the photo-generated carriers and photons, as shown in Fig. 2(b) [28]. To avoid optical absorption at 930 nm, the InGaAs QWs with a gain peak at 980 nm are placed in the nodes of the 930 nm standing-wave pattern; additionally, the GaAsP layer acts as a barrier to prevent the carrier diffusion generated by the pump [29]. The DBR is grown on the active region, and pairs of GaAs/AlAs layers are used to improve the heat dissipation of DBR.

After the wafers are grown, they are cut into 3 × 3 mm^2 chips and soldered onto diamond heat-spreaders. Next, the 300 μm GaAs substrate must be removed. First, mechanical thinning is used to remove ~200 μm of the substrate. The remaining substrate thickness is removed via selective chemical etching. A solution of aqueous ammonia and hydrogen peroxide in the ratio of 1:20 is used as a corrosive. A GaInP corrosion barrier layer on the surface of the gain chip ensures that the gain-chip structure is not damaged when the substrate is removed. An anti-reflective coating is then deposited on the gain chip to improve its emitting efficiency. The heat-spreaders are subsequently mounted on the heat sink with the TEC for cooling.

3. Results

The reflectivity spectrum of the gain chip after removal of the substrate is shown in Fig. 3. Two dips, located at 948 and 997 nm, can be observed in the reflectivity band, which represent the resonance wavelengths of the Fabry–Perot (FP) cavity [30]. The FP dip at 948 nm is deeper than that at 997 nm. Thus, the optical phase match within the gain chip at 948 nm is considerably better. The maximum value in the reflectivity spectrum reaches nearly 100%, which indicates the high reflectivity of the DBR structure.

By pumping the gain chip at a low power level, the photoluminescence (PL) spectrum of the gain chip is recorded at the front and edge of the gain chip; the results are shown in Fig. 3. Two PL peaks, at 945 and 992 nm, can be observed in the PL spectrum recorded on the plane of the gain chip. This is consistent with the FP dips in the reflectivity spectrum. This can be attributed mainly to the fact that the output PL spectrum from the gain-chip surface is modulated by the FP cavity formed by the active region and DBR structure. The PL intensity at 945 nm is considerably higher than that at 992 nm. This results in a higher output efficiency near 945 nm at a lower pump power.

The PL spectrum in the edge direction is also shown in Fig. 3. This spectrum provides information on the emission of the QWs, which is unmodified by the FP cavity. Two major peaks with nearly the same intensity are observed. The peak wavelengths, originating from the two sets of QWs, are located at 928 and 975 nm. The full-width-at-half-maximum (FWHM) of the PL spectrum with the longer peak wavelength is considerably wider than that of the spectrum with shorter wavelength. The wider FWHM of the wider-well (lower energy and longer-wavelength) PL is primarily because of the lesser degree of quantum confinement of the carrier, as opposed to the narrower well. The PL spectra with lower energy indicates optical transition from the light-hole to the first conduction band. For QWs with longer peak wavelengths, the pump light exhibits a strong well pumping effect. In-well pumping can transport more carriers to the subbands in the valence and conduction bands. Thus, the FWHM of the PL spectrum can be increased by combining the PL generated from different energy levels.

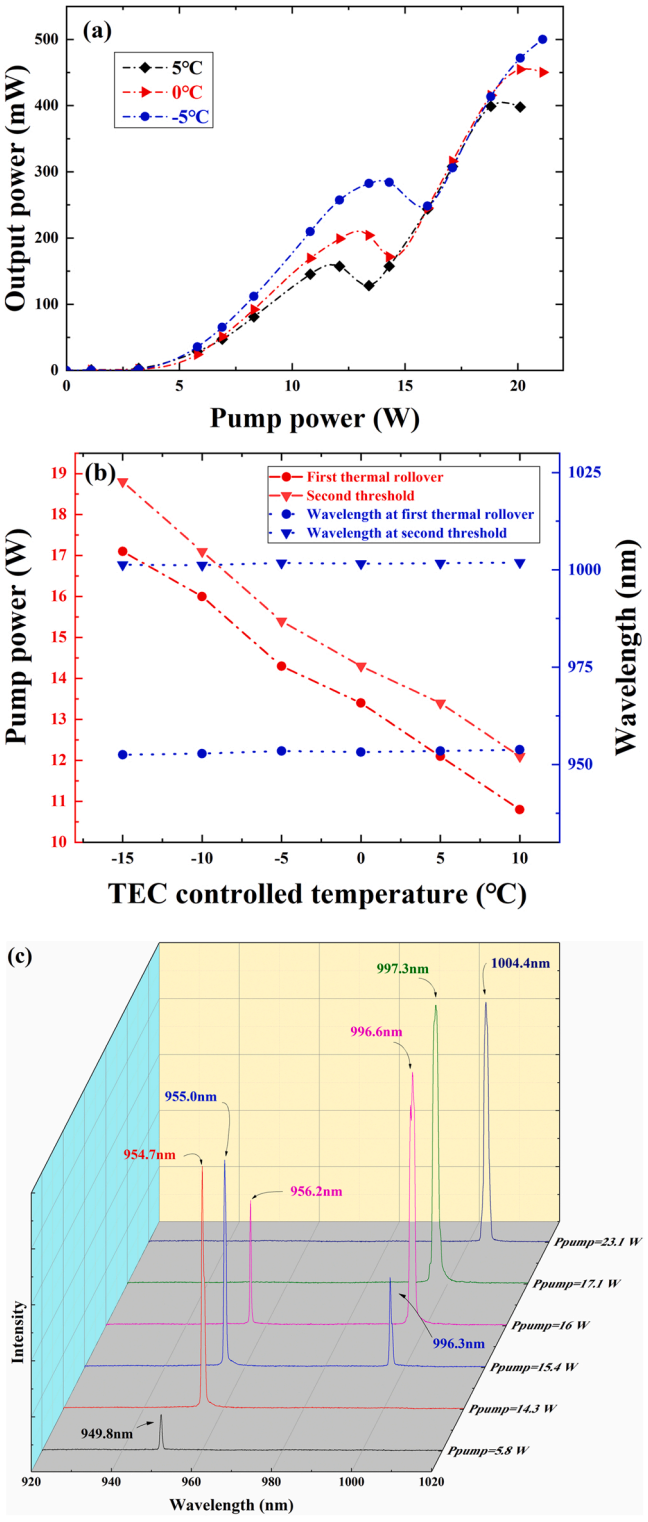

Fig. 5. (a) Variation in output power with pump power at heat-sink temperatures of –5, 0, and 5 °C. (b) Variation in first rollover power and second threshold power with the heat-sink temperature, and the corresponding emitted wavelengths. (c) Variation in lasing wavelength with pump power at −5 °C.

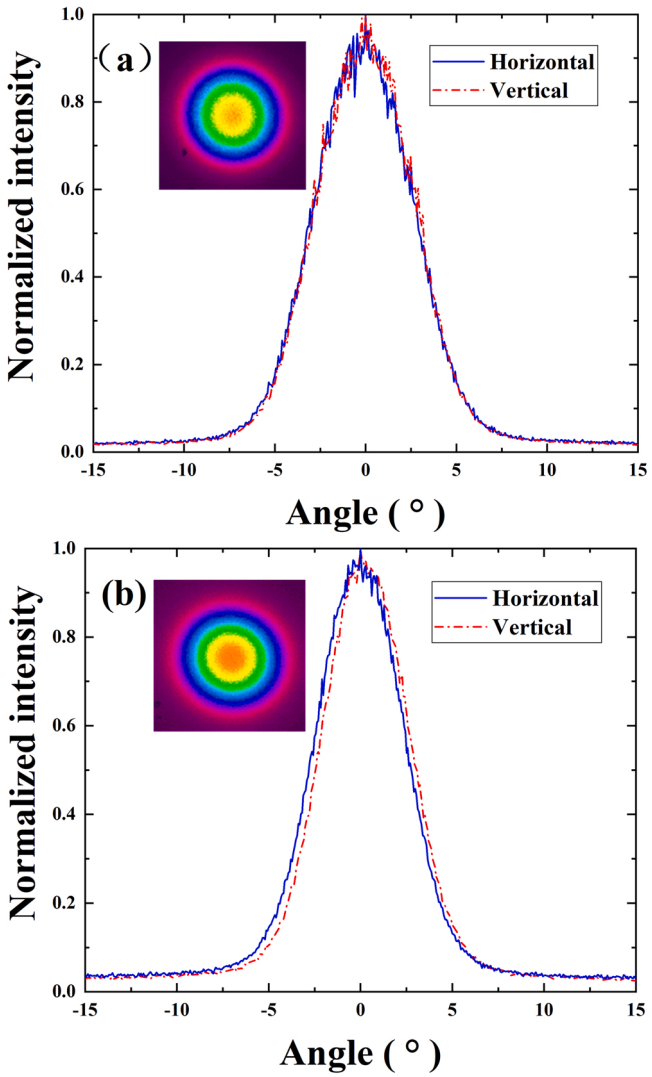

Fig. 6. One-dimensional far-field patterns of the VECSEL measured under pump powers of (a) 8.3 W and (b) 14.3 W. The heat sink temperature is controlled at −5 °C. Inset: Beam profiles from the VECSEL.

The PL spectra at the front of the gain chip, at different pump powers, were measured with the TEC controlled at − 5 °C; the results are shown in Fig. 4. Two PL peaks can be observed at 945 and 992 nm (Fig. 3). As the pump power increases, the temperature of the active region rises. Thus, the PL peaks redshift slightly. The intensity of the two PL peaks also increases with the pump power. The peak at 945 nm is much more intense than that at 992 nm when the pump power is lower than 14.3 W. As the pump power is increased, the intensity of the peak at 992 nm exceeds that of the peak at 945 nm. This phenomenon is caused mainly by the rapid redshift of the gain spectra of the QWs. The temperature redshift coefficient of the gain spectra is nearly three times that of the cavity mode [31]; therefore, as the pump power increases, the PL peak from the surface of the gain chip shifts to the second FP cavity mode.

Fig. 5(a) shows the output power of the output coupling mirror, with a transmission rate of 3%, as a function of the power of pump source, for radiator temperatures of − 5, 0, and 5 °C. The gain chip pump light absorption efficiency is ~75%. Fig. 1 shows the experimental configuration used. The two ranges over which the output power is linearly dependent on the pump power can be observed. The power rollover between the two ranges can also be observed from the power curve. A wavelength difference of nearly 50 nm between the emitted wavelengths appears at different heat-sink temperatures, as shown in Fig. 5(b) and 5(c). As shown in Fig. 5 (b), the pump power, at both the first thermal rollover point and the second threshold (concave point of power curve), decreases as the operating temperature is increased. The first thermal rollover point refers to the first inflection point in the power curve. With the increase in pump power, the first wavelength redshift is higher and the cavity mode is gradually detuned, consequently increasing the temperature in the active region and decreasing the output power. The second threshold indicates the threshold of the second wavelength. With the second wavelength redshift matching the cavity mode, the carrier deposited in the active region decreases and the output power increases with the second wavelength lasing. Thus, thermal effect is the main reason for the change in wavelength.

This corresponds to the change in PL with pump power, as depicted in Fig. 4. However, the separation of the two emitted wavelengths, at different temperatures, remains almost unchanged.

The lasing wavelengths under different pump powers at the heat-sink temperature of − 5 °C are shown in Fig. 5(c). Different lasing wavelengths can be observed near the power rollover. The first power curve at a lower pump power corresponds to the emission at ~955 nm. In this emission state, the maximum output power is ~280 mW at − 5 °C, as shown in Fig. 5(a). The pump power continues to increase, resulting in thermal inversion of the emission at the first wavelength; moreover, a second threshold appears, leading to the emission at the second wavelength, which is ~997 nm. The maximum output power at this wavelength exceeds 500 mW. With further increase in the pump power, the emission wavelength can reach 1004.4 nm. The second wavelength appears at the pump power of 15.4 W. With increasing pump power, the temperature of the active region increases. The wavelength drift with temperature leads to a more accurate cavity mode matching of the second wavelength compared with that of the first wavelength. Thus, the output of the second wavelength will increase and that of the first wavelength will decrease; when the pump power exceeds 16 W, the first wavelength disappears. Therefore, dual-wavelength emission for pump powers of 15.4–16 W is possible. The output power under dual-wavelength emission can reach nearly 250 mW for a pumping power of 16 W. Moreover, the relative intensity between the two emission wavelengths can be controlled effectively by varying the pump power.

The far-field pattern of the developed VECSEL is shown in Fig. 6 at an operating temperature of − 5 °C. Fig. 6(a) shows the far-field pattern under a pumping power of 8.3 W. The emission wavelength is 955 nm, and the divergence angles of the FWHM along the two orthogonal directions, at this wavelength, are 6.93° and 6.48°. The far-field pattern under a pumping power of 14.3 W is shown in Fig. 6(b). Dual-wavelength lasing can be observed under this pumping power, as shown in Fig. 5(b). The far-field patterns also show a two-dimensional Gaussian cross-section. The divergence angles are 7.72° and 7.16°.

4. Conclusions

With a specially designed gain chip consisting of QWs with two different gain wavelengths, we fabricated a high-power VECSEL with switchable emitting wavelengths. The gain-chip structure with two cavity modes enables effective switching of the lasing wavelength between 955 and 997 nm. This VECSEL with a dual-wavelength output in the same cavity on the same chip can generate output in the terahertz band through nonlinear crystal differential frequency. Its unique compact cavity and high power output are obvious advantages in the generation of the terahertz band. Output powers of VECSEL exceeding 280 and 500 mW were achieved at emission wavelengths of 955 and 1004 nm, respectively. Moreover, dual-wavelength emission with an output power of more than 250 mW was demonstrated under specific pumping powers. These results highlight the potential of VECSELs for wavelength-switching and difference frequency terahertz-wave generation.

Funding

This research was funded by the National Key Research and Development Program of China (Grant No. 2018YFB2002401), and the National Natural Science Foundation of China (Grant No. 61874117, 11774343, 61874119, 61991433).

Declaration of Competing Interest

The authors declare that they have no known competing financial interests or personal relationships that could have appeared to influence the work reported in this paper.

References

[1] A. Giesen, J. Speiser, Fifteen years of work on thin-disk lasers: results and scaling laws, IEEE J. Sel. Top. Quantum Electron 13 (2007) 598–609, https://doi.org/10.1109/JSTQE.2007.897180.
[2] C. Hessenius, M. Lukowski, J. Moloney, M. Fallahi, Tunable single-frequency yellow laser for sodium guidestar applications, SPIE Newsroom (2012), https://doi.org/10.1117/2.1201202.004115.
[3] F. Wang, X. Wang, Analysis on thermal characteristics of annular beam pumped vertical-external-cavity surface-emitting lasers by finite element method, Optik 125 (2014) 5719–5722, https://doi.org/10.1016/j.ijleo.2014.06.032.
[4] K. Nechay, A. Mereuta, C. Paranthoen, et al., IEEE J. Quantum Electron (2020), https://doi.org/10.1109/JQE.2020.2986770.
[5] M. Gaulke, J. Heidrich, B.Ö. Özgür Alaydin, et al., High average output power from a backside-cooled 2-μm InGaSb VECSEL with full gain characterization, Opt. Express 29 (2021) 40360–40373, https://doi.org/10.1364/OE.438157.
[6] T. Schwarzbäck, H. Kahle, M. Eichfelder et al., Generation of UV Laser Light via Intra-Cavity Frequency Doubling of an AlGaInP-VECSEL, Lasers & Electro-Optics Europe, IEEE Publications, 2011. https://doi.org/10.1109/cleoe.2011.5942573.
[7] T. Leinonen, Y.A. Morozov, A. Harkonen, M. Pessa, Vertical external-cavity surface-emitting laser for dual-wavelength generation, IEEE Photon. Technol. Lett. 17 (2005) 2508–2510, https://doi.org/10.1109/LPT.2005.859483.
[8] T.A.G. Bondaz, A. Laurain, J.V. Moloney, J.G. McInerney, Generation and stabilization of continuous-wave THz emission from a bi-color VECSEL, IEEE Photonics Technol. Lett. 31 (2019) 1569–1572, https://doi.org/10.1109/LPT.2019.2938169.
[9] A.S. Thampy, M.S. Darak, S.K. Dhamodharan, Phys. E Low Dimens. Syst. Nanostruct. (2015), https://doi.org/10.1016/j.physe.2014.09.023.
[10] K.E. Peiponen, P. Silfsten, J. Pajander, J. Ketolainen, Broadening of a THz pulse as a measure of the porosity of pharmaceutical tablets, Int. J. Pharm. 447 (2013) 7–11, https://doi.org/10.1016/j.ijpharm.2013.02.041.
[11] F. Hindle, A. Cuisset, R. Bocquet, G. Mouret, Continuous-wave terahertz by photomixing: applications to gas phase pollutant detection and quantification, C.R. Phys. 9 (2008) 262–275, https://doi.org/10.1016/j.crhy.2007.07.009.
[12] Z. Lu, X. Liu, Y. Pan, et al., Application of terahertz technology in cooperative detection of space targets. 9th UK-Eur.-China Workshop on Millimetre Waves and Terahertz Technologies (UCMMT), IEEE Publications, 2016, pp. 202–205, https://doi.org/10.1109/UCMMT.2016.7874011.

[13] G. Brévalle, S. Pes, C. Paranthoën, et al., Direct measurement of the spectral dependence of Lamb coupling constant in a dual frequency quantum well-based VECSEL, Opt. Express 27 (2019) 21083–21091, https://doi.org/10.1364/OE.27.021083.
[14] H. Guoyu, C. Kriso, F. Zhang, et al., Two-chip power-scalable THz-generating semiconductor disk laser, Opt. Lett. 44 (2019) 4000–4003, https://doi.org/10.1364/OL.44.004000.
[15] K.A. Fedorova, H. Guoyu, M. Wichmann, et al., Widely tunable terahertz-generating semiconductor disk laser, Phys. Status Solidi RRL 14 (2020), https://doi.org/10.1002/pssr.202000204.
[16] M. Scheller, C.W. Baker, S.W. Koch, et al., High power dual-wavelength VECSEL based on a multiple folded cavity, IEEE Photon. Technol. Lett. 29 (2017) 790–793, https://doi.org/10.1109/LPT.2017.2685595.
[17] A. Hamadou, J.-L. Thobel, S. Lamari, Dynamic modeling of a terahertz quantum cascade laser based on difference frequency generation, Optik 156 (2018) 596–605, https://doi.org/10.1016/j.ijleo.2017.11.126.
[18] Fangsen Xie Shijia Zeng, Z. Rao, Theoretical analysis of difference frequency generation for terahertz generation in a sheet microcavity from the CO_2 laser, Optik 172 (2018) 1111–1116, https://doi.org/10.1016/j.ijleo.2018.07.130.
[19] H. Guoyu, K.A. Fedorova, C. Kriso, et al., Room-temperature CW THz-emitting two-chip semiconductor disk laser, Int. Conf. Laser Opt. (ICLO) 2020 (2020), https://doi.org/10.1109/ICLO48556.2020.9285617.
[20] M. Scheller, J.M. Yarborough, J.V. Moloney, et al., Room temperature continuous wave milliwatt terahertz source, Opt. Express 18 (2010) 27112–27117, https://doi.org/10.1364/OE.18.027112.
[21] A. Laurain, R. Rockmore, I. Kilen, et al., VECSEL platform for single/dual frequency CW operation and ultrashort pulse generation. IEEE International Semiconductor Laser Conference (ISLC), IEEE Publications, 2018, https://doi.org/10.1109/ISLC.2018.8516186.
[22] H. Kogelnik, T. Li, Laser beams and resonators, Appl. Opt. 5 (1966) 1550–1567, https://doi.org/10.1364/AO.5.001550.
[23] M. Kuznetsov, F. Hakimi, R. Sprague, et al., Design and characteristics of high-power (> 0.5-W CW) diode-pumped vertical-external-cavity surface-emitting semiconductor lasers with circular TEM/sub00/ beams, IEEE J. Sel. Top. Quantum Electron. 5 (1999) 561–573, https://doi.org/10.1109/2944.788419.
[24] E. Tournié, K.H. Ploog, C. Alibert, 47In0. 53As quantum wells: a new III-V materials system for light emission in the mid-infrared wavelength range. InAs/Ga, Appl. Phys. Lett. 61 (0) (1992) 2808–2810, https://doi.org/10.1063/1.108044.
[25] Y. Wang, X. Sheng, Q. Guo, et al., Photoluminescence study of the interface fluctuation effect for InGaAs/InAlAs/InP single quantum well with different thickness, Nanoscale Res. Lett. 12 (2017) 229, https://doi.org/10.1186/s11671-017-1998-8.
[26] E. Kantola, T. Leinonen, S. Ranta, et al., High-efficiency tunable yellow-orange VECSEL with an output power of 20 W, Proc. SPIE 8966 (2014) 89660D, https://doi.org/10.1117/12.2037676.
[27] A. Jasik, A.K. Sokół, A. Broda, et al., Dual-wavelength vertical external-cavity surface-emitting laser: strict growth control and scalable design, Appl. Phys. B 122 (2016), https://doi.org/10.1007/s00340-015-6307-6.
[28] Y.A. Morozov, T. Leinonen, A. Harkonen, M. Pessa, Simultaneous dual-wavelength emission from vertical external-cavity surface-emitting laser: a numerical modeling, IEEE J. Quantum Electron 42 (2006) 1055–1061, https://doi.org/10.1109/JQE.2006.881723.
[29] Y.A. Morozov, I.S. Nefedov, T. Leinonen, M.Y. Morozov, Nonlinear-optical frequency conversion in a dual-wavelength vertical-external-cavity surface-emitting laser, Semiconductors 42 (2008) 463–469, https://doi.org/10.1134/S1063782608040167.
[30] H.D. Yang, C. Lu, R. Hsiao, et al., Characteristics of MOCVD- and MBE-grown InGa(N)As VCSELs, Semicond. Sci. Technol. 20 (2005) 834–839, https://doi.org/10.1088/0268-1242/20/8/035.
[31] A.C. Tropper, S. Hoogland, Extended cavity surface-emitting semiconductor lasers, Prog. Quantum Electron. 30 (2006) 1–43, https://doi.org/10.1016/j.pquantelec.2005.10.002.